NRL Report 7945

The Effects of Vortex Coherence, Spacing, and Circulation on the Flow-Induced Forces on Vibrating Cables and Bluff Structures

S. E. Ramberg and O. M. Griffin

Applied Mechanics Branch
Ocean Technology Division

January 2, 1976

NAVAL RESEARCH LABORATORY
Washington, D.C.

Approved for public release; distribution unlimited.

SECURITY CLASSIFICATION OF THIS PAGE (When Data Entered)

REPORT DOCUMENTATION PAGE

READ INSTRUCTIONS BEFORE COMPLETING FORM

1. REPORT NUMBER
NRL Report 7945

2. GOVT ACCESSION NO.

3. RECIPIENT'S CATALOG NUMBER

4. TITLE (and Subtitle)
THE EFFECTS OF VORTEX COHERENCE, SPACING, AND CIRCULATION ON THE FLOW-INDUCED FORCES ON VIBRATING CABLES AND BLUFF STRUCTURES

5. TYPE OF REPORT & PERIOD COVERED
Interim report on a continuing NRL Problem

6. PERFORMING ORG. REPORT NUMBER

7. AUTHOR(s)
S. E. Ramberg and O. M. Griffin

8. CONTRACT OR GRANT NUMBER(s)

9. PERFORMING ORGANIZATION NAME AND ADDRESS
Naval Research Laboratory
Washington D.C. 20375

10. PROGRAM ELEMENT, PROJECT, TASK AREA & WORK UNIT NUMBERS
NRL Problem F02-36
Project YF 53.535.004.02.002

11. CONTROLLING OFFICE NAME AND ADDRESS
Naval Facilities Engineering Command
Alexandria Va. 22332

12. REPORT DATE
January 2, 1976

13. NUMBER OF PAGES
35

14. MONITORING AGENCY NAME & ADDRESS(if different from Controlling Office)
Civil Engineering Laboratory
Naval Construction Battalion Center
Port Hueneme, Ca. 93043

15. SECURITY CLASS. (of this report)
UNCLASSIFIED

15a. DECLASSIFICATION/DOWNGRADING SCHEDULE

16. DISTRIBUTION STATEMENT (of this Report)
Approved for public release; distribution unlimited

17. DISTRIBUTION STATEMENT (of the abstract entered in Block 20, if different from Report)

18. SUPPLEMENTARY NOTES

19. KEY WORDS (Continue on reverse side if necessary and identify by block number)
Flow-induced vibrations
Vortex shedding
Cable strumming
Marine mooring systems
Laminar and turbulent wakes

20. ABSTRACT (Continue on reverse side if necessary and identify by block number)

The vortex wake of a vibrating flexible cable was studied by means of velocity measurements and correlation, frequency spectra, and flow visualization. Three distinct spanwise regimes were identified according to wake structure. Near the cable nodes the flow resembles that of a stationary cable. Adjacent to the node is a transition regime which extends up to the locked-in or synchronized wake flow about the cable antinode. Each regime was characterized by spectral content, degree of spanwise correlation, and local vortex street geometry. Measured downstream velocity profiles and

Continued

DD FORM 1 JAN 73 1473 EDITION OF 1 NOV 65 IS OBSOLETE
S/N 0102-014-6601

SECURITY CLASSIFICATION OF THIS PAGE (When Data Entered)

20. (Abstract continued)

vortex spacing were matched with a mathematical model to obtain the vortex strength and its relation to cable vibration conditions. The von Karman drag formula was used to compute the steady drag coefficients directly, and the distributions of fluctuating lift and drag were inferred from the data. The vortex strength and fluid forces on the vibrating cable were found to be as much as 65 percent larger for locked-in conditions than in the stationary case. Where comparisons were possible, there was good agreement between present results and previous results for vortex-excited rigid cylinders, including some direct measurements of the increased drag.

CONTENTS

INTRODUCTION 1

RELATED INVESTIGATIONS 1

EXPERIMENTAL SYSTEMS AND METHODS 3

Correlation Measurements 4
Spectral Measurements 5
Flow Visualization 5

RANGE OF THE EXPERIMENTS 5

SPANWISE CORRELATION AND SPECTRAL CONTENT IN THE NEAR WAKE 6

VORTEX SPACING 12

THE VELOCITY FIELD OF THE VORTEX WAKE 16

A MATHEMATICAL MODEL FOR THE VORTEX STREET . . . 17

MODEL COMPUTATIONS OF VORTEX STRENGTH AND SPACING 21

VORTEX-INDUCED DRAG 25

SOME COMPARISONS WITH THE DRAG ON VIBRATING RIGID CYLINDERS 26

SUMMARY AND CONCLUSIONS 29

REFERENCES 30

THE EFFECTS OF VORTEX COHERENCE, SPACING, AND CIRCULATION ON THE FLOW-INDUCED FORCES ON VIBRATING CABLES AND BLUFF STRUCTURES

INTRODUCTION

If one of the natural frequencies of a bluff body immersed in a moving stream of fluid is near the frequency at which vortices are naturally shed from the body, then self-excited resonant vibrations can occur if the damping of the system is sufficiently low. There is also a range of frequencies near this so-called Strouhal frequency of vortex shedding over which forced vibrations of the body cause the vortex frequency to be captured by, or to synchronize with, the body frequency. This means that the body and wake have the same characteristic frequency and that the Strouhal frequency, relating to the vortex shedding from a stationary body, is suppressed. The forces which act on a structure are amplified as a result of such vibrations, and these forces are closely related to the changes which occur in the wake flow downstream of the body.

Most early investigations [1-6] of this synchronization or *lock-in* phenomenon dealt with vibrating rigid cylinders, since the wakes of these bodies are nominally two dimensional and are more readily compared to typical stationary-cylinder results [7-12]. More recently the authors examined the wake flow behind a vibrating flexible cable [13,14], where the wake is three dimensional due to the variation of the vibration amplitude along the body span. So far as was possible, a comparison was made between results obtained for those segments of the cable that were resonantly vibrating and corresponding results obtained with vibrating cylinders. In the present report all of the regimes of a vibrating cable's wake are considered, with emphasis on the wake flow near the node. The purposes of the present study are to further investigate the applicability of rigid-cylinder results by a direct comparison of vortex-strength and drag measurements and to gain further insights into the distribution of the time-dependent fluid forces and the near-wake flow. Finally in this report the resulting fluid force distribution is discussed in relation to known cable vibration characteristics in order to determine the applicability of certain simplifying approximations in modeling the vortex-induced response of flexible structures.

RELATED INVESTIGATIONS

In one of the early studies of wakes of vibrating rigid cylinders Koopmann [1] showed that frequency locking between the wake and the cylinder occurs within a range of ±25-30 percent of the Strouhal shedding frequency. Both Koopmann and Griffin [2] observed the increased correlation or coherence of the shedding along the cylinder for forced oscillations greater than about 10 percent of a cylinder diameter. Additional evidence of this phenomenon was given by Ferguson and Parkinson [3] by means of

Manuscript submitted October 20, 1975.

pressure correlations in the wake and on the surface of an oscillating cylinder. Toebes [4] later examined the correlation of velocity fluctuations and base pressure near a forced vibrating cylinder at high Reynolds numbers near 10^4 or 10^5. Earlier work by Roshko [7], Bloor [8], Bloor and Gerrard [9], and Shaefer and Eskinazi [10] provided basic information about the structure of the vortex wake of a stationary cylinder that serves as a basis for comparison.

Information on the strength of vortices is sparse for stationary bodies, and only one study is known to have considered the effects of rigid-cylinder vibrations on vortex strength [15]. The introduction of transverse vibrations, either vortex-excited or forced, into the body-wake system increases the complexities involved in any attempt to determine such wake parameters as vortex strength and spacing, since these parameters depend on the length of the vortex formation region and on the distance from the end of the formation region to a measurement point in the wake. The investigations by Griffin [2], Griffin and Votaw [5], and Griffin [6] have explored the dependence of the formation-region length and wake structure behind rigid cylinders on the amplitude and frequency of vibration. These experiments also showed that the formation length is an appropriate scaling length for the vortex wake of an oscillating bluff body.

With this fundamental background the authors initiated the investigation of the three-dimensional vortex wake behind a vibrating flexible cable because of its practical importance in the modeling of the flow-induced vibrations of undersea cables and other flexible bluff structures. It was observed [13] that the length of formation is related to the amplitude and frequency of the vibratory motion in much the same way as had been found for rigid cylinders. Similarly the remaining downstream wake structure can be scaled by this formation length, and doing so yields comparably scaled rms and mean velocity distributions.

Also, the magnitude of the correlation of the shedding, the vortex spacing, and the vortex convection speed were virtually indistinguishable from corresponding vibrating cylinder results [14] over the spanwise portion of the wake where the cable and vortex frequencies were locked together. Since the flexible cylinder wake is three dimensional, the agreement of results is based on a correspondence between the wake behind a *single* point on the cable and the two-dimensional wake of a rigid cylinder vibrating at the same Reynolds number, frequency, and amplitude. Consequently the length of formation varies along the cable span and directly reflects the amplitude distribution.

These results however are limited in that the amplitude along the cable eventually drops below the threshold (approximately 10 percent of a diameter) usually associated with the frequency-locking phenomenon. In the region between this point and the node of the cable, the analogy between the cable and the rigid-cylinder wakes breaks down. The purpose of the present report is thus to examine the flow field near the nodal region of the cable, the region of resonant vibrations where the wake and body frequencies are locked together, and finally the transition region adjacent to the node where the vibration amplitude is below the frequency-locking threshold.

EXPERIMENTAL SYSTEMS AND METHODS

The experiments reported here were performed in an open jet wind tunnel (Fig. 1) with a 150-mm-square exit preceded by a 20:1 contraction section. Two DISA hot-wire anemometers (55D05) with low-interference probes (55F01) were used for the flow measurements, and the outputs from the anemometers were linearized in the speed range 0.25 to 7.0 m/s. The linearized velocity signals were processed by a DISA analog correlator (55D70) to obtain a crosscorrelation function. The test cable for the experiments was a length of solid rubber cord with a nominal diameter d of 3.3 mm which spanned the exit section in such a way that a full standing wave of length L could be generated inside the flow. In practice the cable was excited in its second mode with the a node centered in the exit section (Fig. 2). The cable Strouhal frequency was adjusted by varying the flow velocity, and the forced excitation of the cable was provided by miniature shakers acting as sinusoidal displacement inputs to each end of the cable. An L/d ratio of about 45 and the use of endplates minimized any three-dimensional effects due to the cable length and the air-jet boundaries.

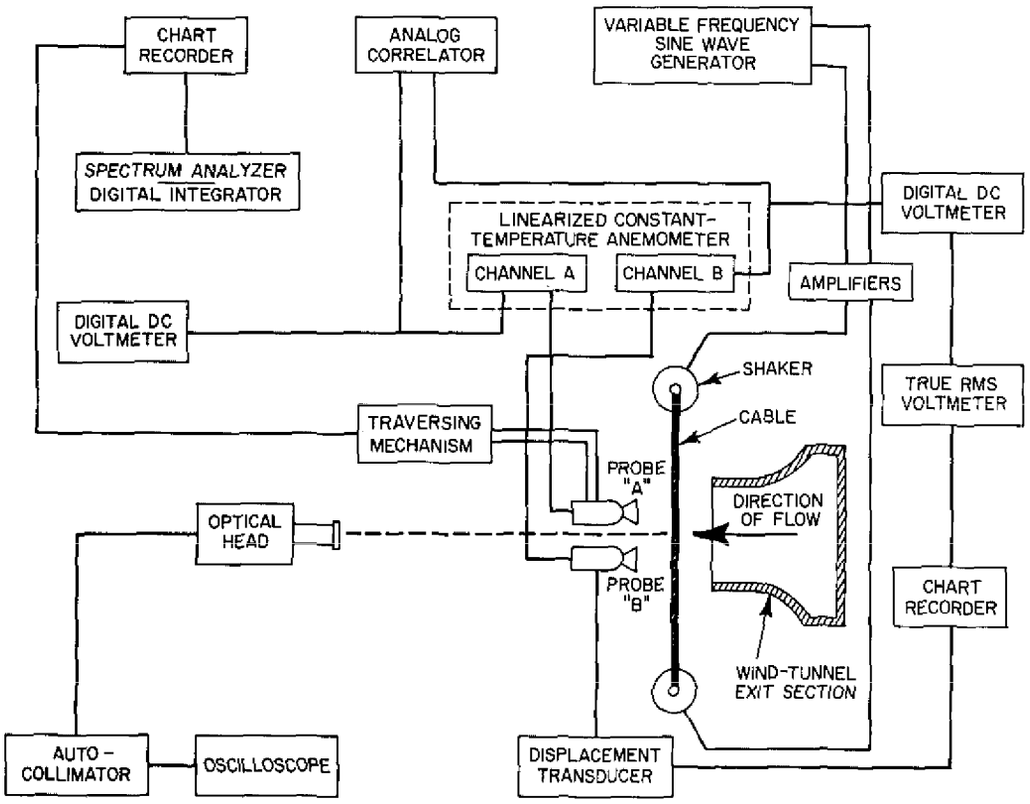

Fig. 1 — Test system

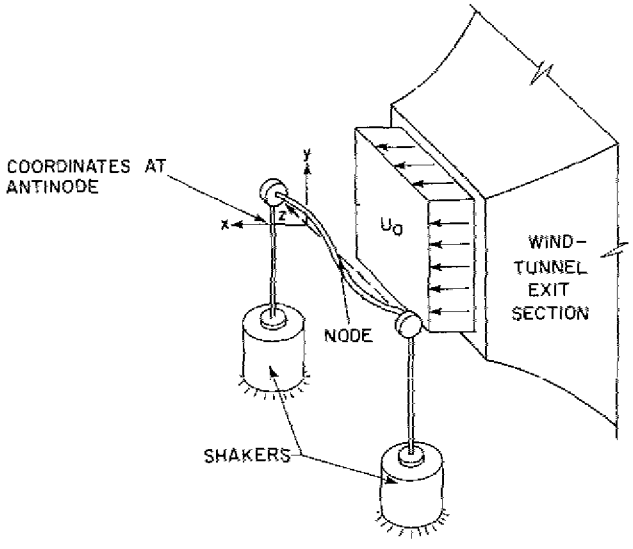

Fig. 2 — Cable specimen and coordinate system at the wind-tunnel exit

The shedding frequency from the stationary cable was determined from the spectrum of the hot-wire signal. All spectral measurements were made with a Honeywell Saicor Spectrum Analyzer/Digital Integrator (Model 51B). The peak-to-peak amplitude of the cable vibration was obtained from a PhysiTech Model 440 Auto-Collimator. The optical head of the collimator was placed about 1 meter directly downstream of the cable and could be swiveled in the plane of the cable to detect the motion at any point across the exit section.

The origin of the coordinate system (Fig. 2) is on the stationary cable axis at a point where the vibrating cable has an antinode. The distance in the mean flow direction is denoted by x, the distance perpendicular to the mean flow and perpendicular to the cable axis is denoted by y, and the distance along the cable axis is denoted by z. The circular cable of diameter d was oscillated in a plane normal to the mean flow from the wind tunnel exit, and the local peak-to-peak amplitude of cable motion is given by $a(z)$, the cable vibration frequency by f, and the vortex shedding or Strouhal frequency of the stationary cable by f_s. The mean velocity measured at the probe is given by U, and the free-stream mean velocity is given by U_0. The fluctuating component of the velocity is denoted by u and represents the instantaneous value measured at the hot-wire probe. More detailed descriptions of the apparatus and calibration procedure are available in Refs. 13 and 14.

Correlation Measurements

The spanwise crosscorrelation coefficient is defined by

$$\rho_{AB}(\Delta z) = \frac{\dfrac{1}{T}\displaystyle\int_0^T u_A(z, t) u_B(z + \Delta z, t)\, dt}{\sqrt{\dfrac{1}{T}\displaystyle\int_0^T u_A(z, t)^2\, dt}\ \sqrt{\dfrac{1}{T}\displaystyle\int_0^T u_B(z + \Delta z, t)^2\, dt}}, \tag{1}$$

where u_A and u_B are the fluctuating velocity signals from the two probes. The spanwise crosscorrelation functions were obtained by placing two adjacent probes behind a cable antinode and traversing the near wake with one probe through the nodal region of the wake and to the other antinode. Previous correlation data for the lock-in region as well as criteria for positioning the probes are available in Ref. 14. Downstream correlations are similarly defined and obtained when the spacial coordinate is x and the traversing probe is moved in the streamwise direction. The result of this procedure, under appropriate conditions, is a measurement of the longitudinal vortex spacing λ.

Spectral Measurements

At any particular location the frequency content of the fluctuating velocity signal was obtained from an integrated (averaged) spectrum of the linearized hot-wire signal. The objective of the measuring and recording system was to provide a linear display of the average amplitude of each contributing frequency, where the averaging was over several (eight to 16 or more) sample spectra. Due to the nature of the lock-in phenomenon, the spectra consisted of a number of spikes related to the two frequencies f and f_s. The characteristic wake length scales are the length of formation ℓ_F and wake width at formation d_F, so that quantitative comparisons of various spectra would require similarity in these scales. Since these scales vary along the cable span, traverses at constant displacements of x and y yield only a qualitative comparison. Hence, no attempt is made to express results on an absolute scale, and spectral components of the fluctuating velocity are normalized with respect to a single arbitrary reference signal. The normalized component amplitudes of the fluctuating velocity signal at the vibration and Strouhal frequencies are thus C_n and C_s respectively, expressed in arbitrary units.

The Flow Visualization System

The vortex wakes were made visible by introducing a sheet of aerosol into the wind tunnel. This technique, in which compressed air is bubbled through di(2-ethylhexyl phthalate), or DOP, produces a chemically inert and nontoxic aerosol which has proved highly effective for the visualization of vortex wake flows. The DOP aerosol was introduced into the flow upstream of the cable from the trailing edge of a movable airfoil positioned in the contraction section of the wind tunnel. In this way a DOP sheet perpendicular to the cable axis could be located at any point along the cable. The strobe lighting system was synchronized with the cable motion to visually confirm the locking-in of the vortex shedding with the vibrations. Except for the movement of the airfoil injector, the visualization system is the same as one which the authors previously described in Refs. 5 and 15. Relative measurements of longitudinal vortex spacing were obtained from the photographs by scaling the size of the anemometer probe in each frame. The actual longitudinal spacing was also directly measured by means of the streamwise correlation technique described at the end of the paragraph containing Eq. (1).

THE RANGE OF THE EXPERIMENTS

The results are presented and discussed in several separate sections. The first contains spanwise correlation and spectral measurements at Reynolds numbers of 480, 525,

570, and 610, corresponding to frequencies f/f_s = 1.10, 1.00, 0.92, and 0.86 respectively. The downstream wake-velocity and vortex-spacing surveys which follow were obtained at Reynolds numbers of 470, 570, 715, and 1300 and at several combinations of frequency and maximum amplitude. In the remaining sections, wake velocity measurements across the cable span are used to compute the vortex strength and spacing and from these to infer the distribution of the steady drag forces as well as the time-dependent lift and drag forces on the cable. Finally, a comparison is made with available measurements of the drag on vibrating bluff cylinders.

SPANWISE CORRELATION AND SPECTRAL CONTENT IN THE NEAR WAKE

Once a vibration frequency and amplitude were established, the amplitude distribution was recorded for the vibrating cable. As one probe traversed the wake from antinode to antinode, the crosscorrelation function between that probe and the stationary probe was determined and recorded. Intermittently the spectral content of the velocity fluctuations was obtained at various positions of the traversing probe. The results are shown in Figs. 3 through 12. Figure 3 represents a composite correlation function and spectral measurement at three Reynolds numbers for a stationary cable. Typical of this situation is the rapid drop in the crosscorrelation coefficient with increased probe spacing [4,14] and a nearly uniform amplitude of fluctuating velocity at the Strouhal frequency. Before considering the effects of cable motion, it is useful to review the characteristics of the correlation and spectral measurements. The crosscorrelation coefficient between unequal frequencies is zero for a sufficient averaging time, whereas between equal frequencies the coefficient varies between -1 and +1, depending on the relative phase of the signals. On the other hand a spectral measurement records *all* frequency information and is insensitive to phase information. Accordingly Fig. 3 demonstrates that the magnitude of the velocity fluctuations is uniform but varies rapidly in phase, as has often been proposed and observed in the literature for stationary cylinders.

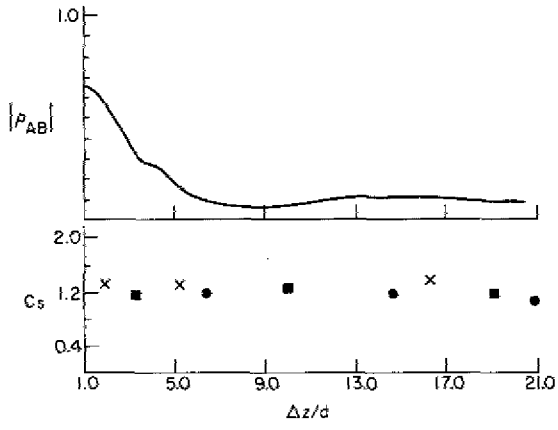

Fig. 3 — Composite spanwise correlogram and spectral component at the Strouhal frequency for a stationary cable at three Reynolds numbers: Re = 525 (●), Re = 570 (■), and Re = 610 (X)

In Fig. 4a, at f/f_s = 0.86 and Re = 610, the maximum amplitude is $a(0)/d$ = 0.08, which is below the threshold of frequency locking for vortex shedding from rigid cylinders. The crosscorrelation coefficient decreases with increased spacing, although not as

rapidly as for the stationary cable, and there is no significant correlation as the nodal region of the wake is traversed. Meanwhile the spectral component C_s at the Strouhal frequency differs from the stationary case in that there is a slight decrease approaching the cable antinodes. A component C_n at the body vibration frequency is introduced which is somewhat smaller than C_s and has a distribution that reflects the distribution in the amplitude of motion. It is likely that the improved correlation is due to an increasingly regular phase relationship of the component C_n at the cable frequency.

The results in Fig. 4b were obtained at the same frequency, but the amplitude was increased sufficiently to place a portion of the cable above the threshold for locking-in between the wake and the vibrations. The correlation function has a constant value (≈ 0.85) about the cable antinode before decreasing to zero at the cable node. Beyond the node the correlation function changes sign (all graphs show only the *modulus* of ρ_{AB}), and about the adjacent antinode a constant value is again attained but at a smaller magnitude of ρ_{AB}. This is not surprising, since a similar effect was observed [14] when two probes were positioned on opposite sides of the wake behind the same half-wave of a cable. Virtually all variations and errors will reduce the measured correlation (particularly for a normalized analog correlation), thus suggesting that these measurements are conservative and indicate a high degree of actual coherence in the shedding. Meanwhile the spectral content has changed markedly in that the component C_s has almost disappeared at the cable antinodes and has increased to its original value near the node. The magnitude of the component C_n at the body vibration frequency is greatly increased at the antinode and continues to reflect the amplitude distribution, including a zero value at the node.

At the same frequency but at a greater amplitude (Fig. 4c) these changes are more pronounced. A larger portion of the cable is above the lock-in threshold, and the magnitude of the correlation is slightly higher. For most of these portions C_s is zero or within the level of background noise but appears to hold its original value at the node. Although C_n does not show a zero at the node, a zero value was observed from the real-time spectral display during the experiments. These observations are consistent with previous work and with the concept of a synchronization or lock-in of the vortex shedding to the body motion.

Figure 5 displays measurements for $f/f_s = 0.92$ and Re = 570, and the results are similar except that the correlation is constant over greater portions of the cable at smaller amplitudes. The lock-in boundary for shedding from rigid cylinders [1] at this frequency is at a much lower amplitude ($\approx 0.1d$) than for the conditions illustrated in Fig. 4 ($\approx 0.25d$). The observed behavior is then as one would expect.

Figure 6 refers to a single experiment at $f/f_s = 1.0$ and Re = 525. Since $C_n = C_s$, little can be determined except the behavior of the correlation ρ_{AB}. The correlation function is constant over a larger span of the cable than would be expected from previous measurements of frequency locking for cylinders, for which the threshold is about $0.1d$. In fact the correlation does not deteriorate until $a/d < 0.07$. Figure 7 was obtained at $f/f_s = 1.10$ and Re = 480 and demonstrates at this higher frequency the same effects that are shown in the previous figures.

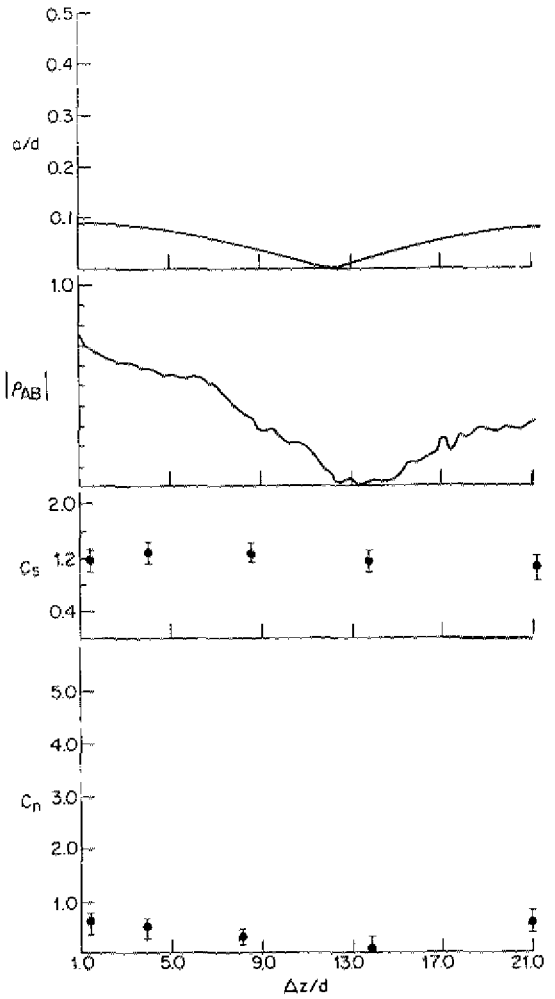

Fig. 4a — Amplitude distribution, spanwise correlogram, and distribution of spectral content at f_s and f for a vibrating cable with $f/f_s = 0.86$, Re = 610, and the maximum amplitude below the frequency-locking threshold

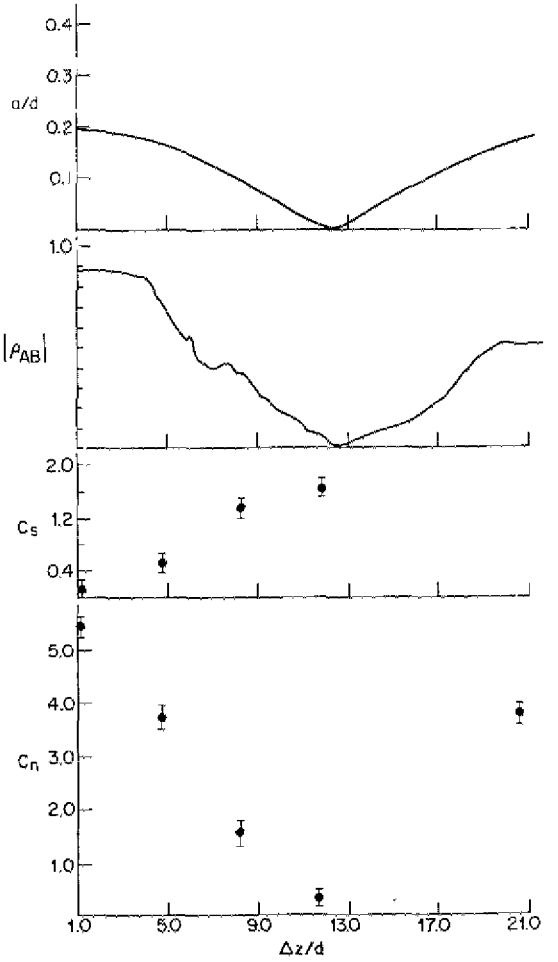

Fig. 4b — Amplitude distribution, spanwise correlogram, and distribution of spectral content at f_s and f for a vibrating cable with $f/f_s = 0.86$, Re = 610, and the maximum amplitude somewhat above the frequency-locking threshold

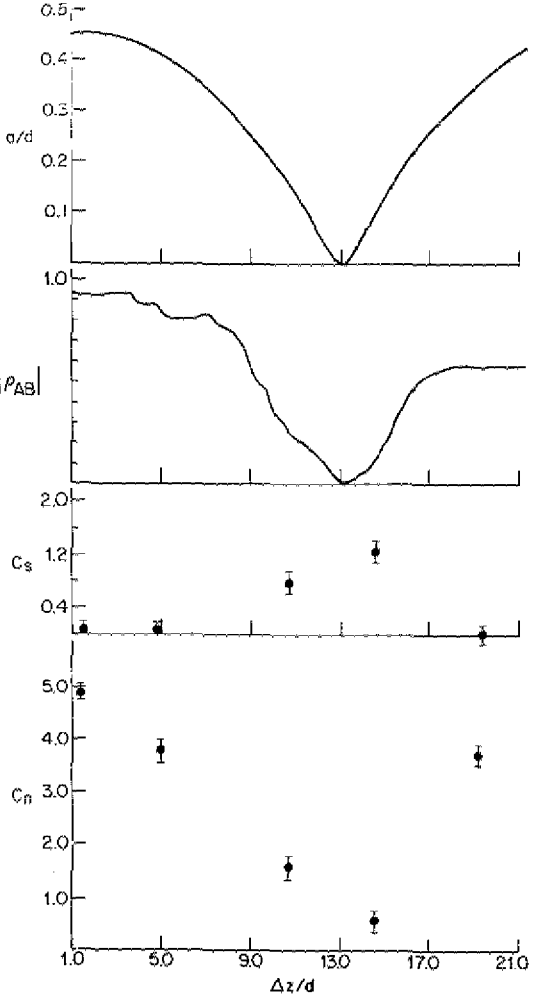

Fig. 4c — Amplitude distribution spanwise correlogram, and distribution of spectral content at f_s and f for a vibrating cable with $f/f_s = 0.86$, Re = 610, and the maximum amplitude considerably above the frequency-locking threshold

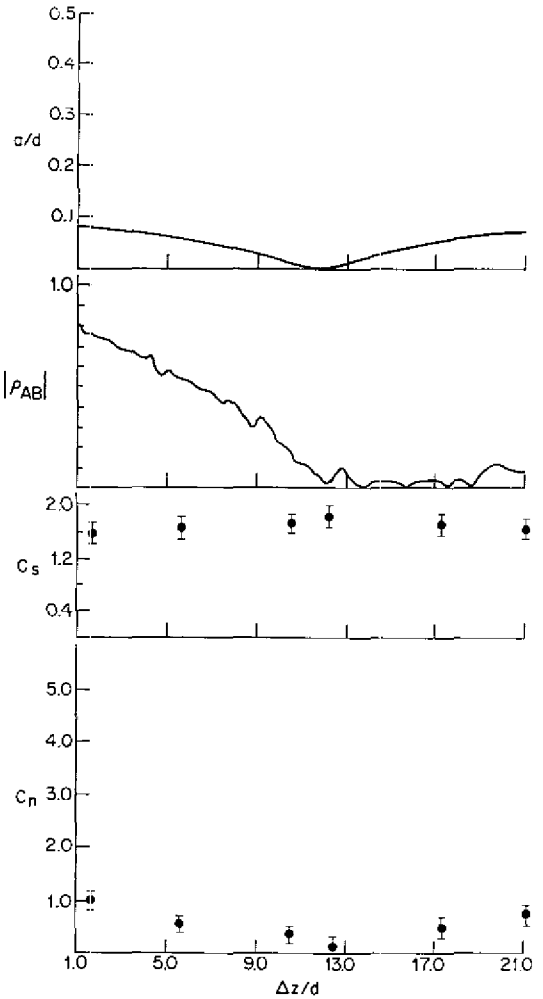

Fig. 5a — Amplitude distribution, spanwise correlogram, and distribution of spectral content at f_s and f for a vibrating cable with f/f_s = 0.92, Re = 570, and the maximum amplitude below the frequency-locking threshold

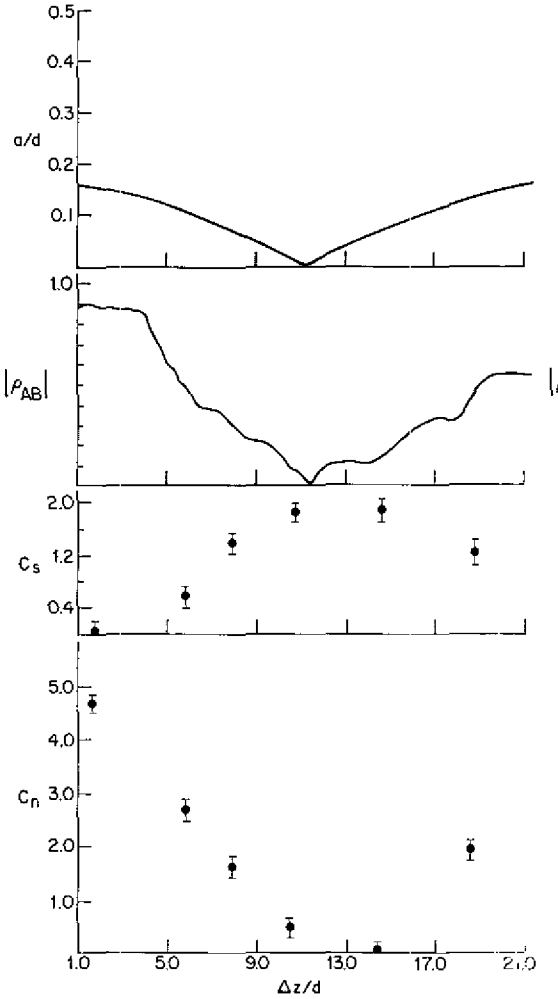

Fig. 5b — Amplitude distribution, spanwise correlogram, and distribution of spectral content at f_s and f for a vibrating cable with f/f_s = 0.92, Re = 570, and the maximum amplitude somewhat above the frequency-locking threshold

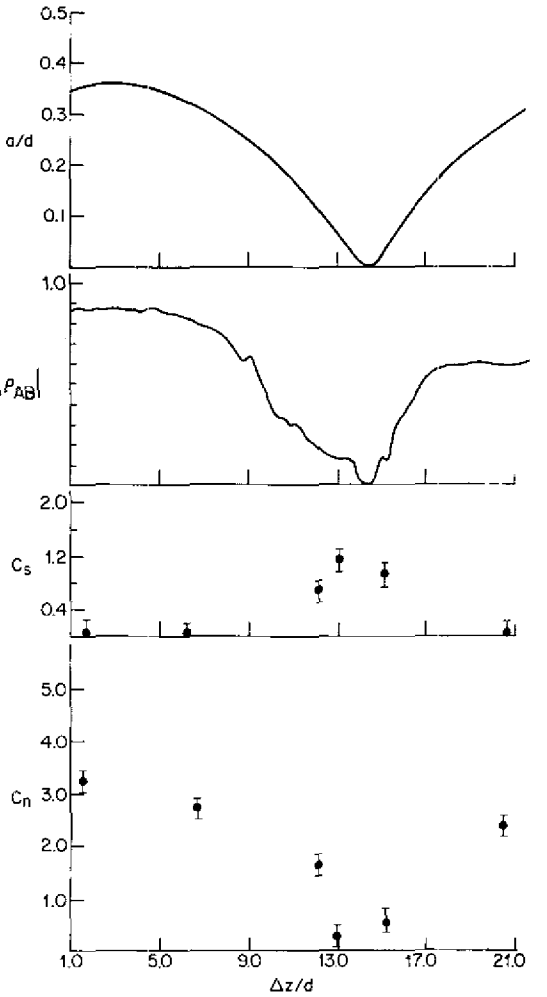

Fig. 5c — Amplitude distribution, spanwise correlogram, and distribution of spectral content at f_s and f for a vibrating cable with f/f_s = 0.92, Re = 570, and the maximum amplitude considerably above the frequency-locking threshold

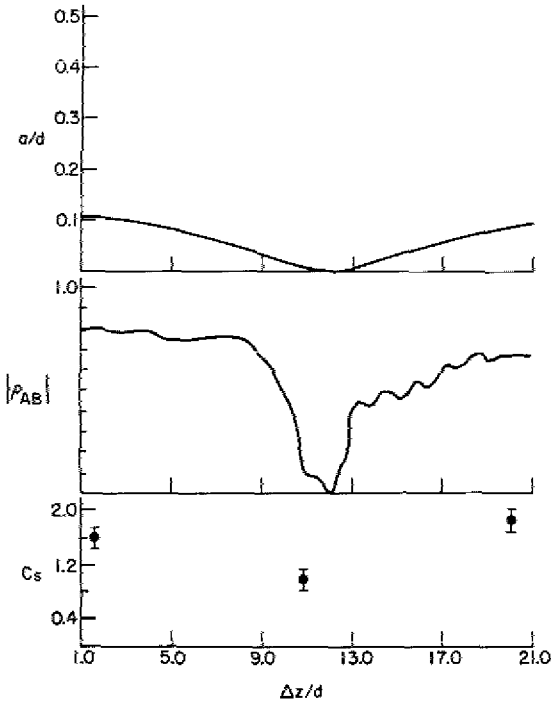

Fig. 6 — Amplitude distribution, spanwise correlogram, and distribution of spectral component at $f_s = f$ for a vibrating cable with $f/f_s = 1.00$ ($C_n = C_s$), Re = 525, and the maximum amplitude slightly above the frequency-locking threshold

The correlograms can be used to determine the frequency-locking boundary for each set of conditions, in that a critical or threshold amplitude corresponding to the rapid drop in correlation can be found for each frequency. However, the existence of two frequencies C_s and C_n implies a certain lack of synchronization. For a cable or other flexible body with a node, the component C_s should exist in the region of the node, whereas there is no such requirement for a rigid cylinder. The lock-in boundaries can then be only approximately equal for the two cases. One would expect that the boundary or, more precisely, the limit of high correlation depends on the relative amplitudes of C_n and C_s along the span of such a flexible body. This is the case, as shown in Table 1, where the critical amplitudes a_t from Figs. 4 through 7 are compared with corresponding rigid-cylinder values and the local ratio of C_n/C_s. A threshold of $C_n/C_s \approx 10$ may be the better of the two definitions for the lock-in boundaries, but the differences are not great.

The data surveyed in Figs. 3 through 7 permit several observations and assertions with regard to the time-dependent fluid force distribution on a vibrating cable. In general there will be fluctuating force components related to both f and f_s (fluctuating lift components f and f_s as well as fluctuating drag components at $2f$ and $2f_s$). Attempts to find any correlation in the components at f_s and $2f_s$ show that they are nearly random and are not likely to contribute to the cable motion. On the other hand there is a regular phase relationship (high correlation) between the fluctuating forces related to the body frequency f over much but *not* all of the cable, and this should be appropriately taken into account in any description of the actual fluid forces. In the following sections the downstream wake structure is investigated to clarify these observations.

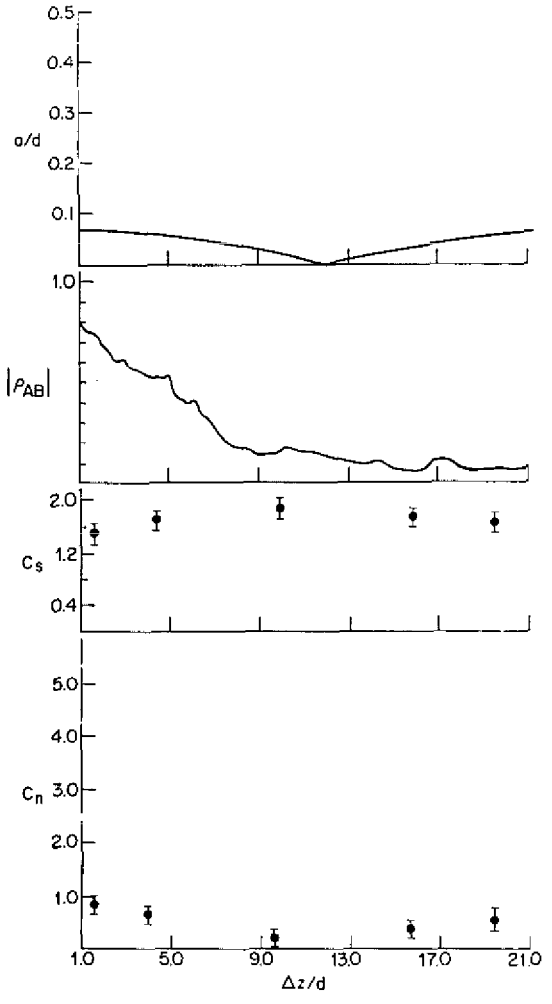

Fig. 7a — Amplitude distribution, spanwise correlogram, and distribution of spectral content at f_s and f for a vibrating cable with f/f_s = 1.10, Re = 480, and the maximum amplitude below the frequency-locking threshold

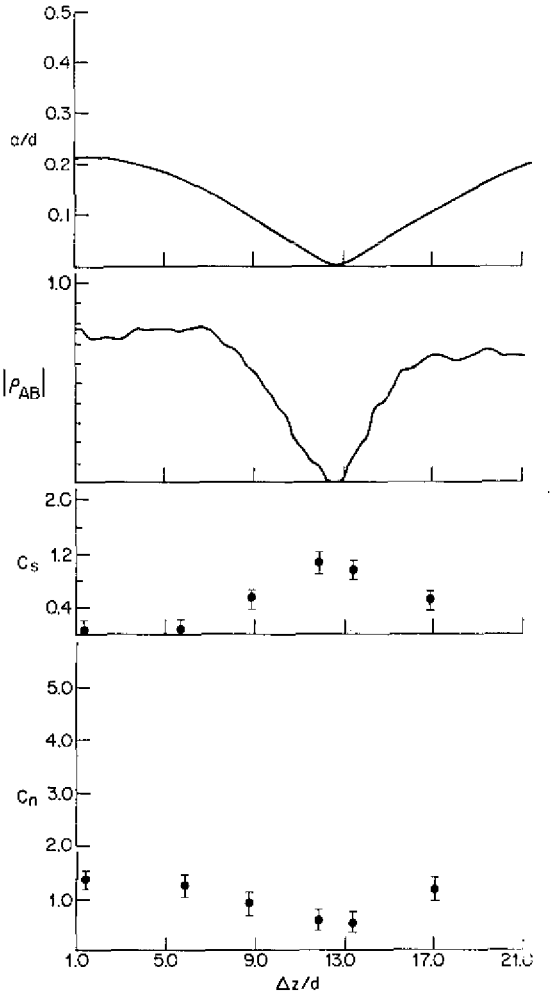

Fig. 7b — Amplitude distribution, spanwise correlogram, and distribution of spectral content at f_s and f for a vibrating cable with f/f_s = 1.10, Re = 480, and the maximum amplitude somewhat above the frequency-locking threshold

Table 1 — A Comparison of the Threshold Amplitudes a_t of Frequency-Locking for Cables (Figs. 4 through 7) and Cylinders

f/f_s	$a(0)/d$	a_t/d		C_n/C_s
		Cable	Cylinder	
0.86	0.20	0.18	0.25	10
0.86	0.46	0.30	0.25	9
0.92	0.16	0.12	0.10	11
0.92	0.36	0.20	0.10	10
1.00	0.11	0.07	0.10	—
1.10	0.21	0.13	0.10	6

VORTEX SPACING

A spacial crosscorrelation in the downstream x direction from a bluff body, at a transverse displacement y which is sufficiently large to negate effects from vortices of opposing sign, yields a periodic function whose wavelength is equal to the longitudinal spacing for vortices of like sign. For vibrating cylinders the longitudinal vortex spacing λ is independent of the amplitude of vibration but appears to be inversely proportional to the vibration frequency at a given Reynolds number [5,15]. This behavior is further substantiated in Fig. 8, where the product (λ/d) (f/f_s) is plotted as a function of Reynolds number for both cables and rigid cylinders. The longitudinal vortex spacing is constant in the x direction, and this is indicative of a constant induced vortex street velocity. The wavelength is then related to the Strouhal number $\mathrm{St} = f_s d/U_0$ by

$$\left(\frac{\lambda}{d}\right)\left(\frac{f}{f_s}\right) = \frac{U_\varphi}{U_0}\,\mathrm{St}^{-1}, \tag{2}$$

where U_φ and U_0 are the vortex-center velocity and free-stream velocity respectively. Experimental values of U_φ/U_0 as determined from the frequency and wavelength are listed in Table 2 and correspond to the points plotted in Fig. 8. Included in the figure are several flagged points corresponding to the experimentally determined values of St^{-1}. From the preceding relation St^{-1} should be proportional to the measured λ/d, and this is the case. As a reference the dashed lines are included in Fig. 8 to show the measured limits of St^{-1} for a stationary circular cylinder. The dashed lines correspond to a smooth cylinder in low-turbulence flow (lower curve) and a rough cylinder in turbulent flow (upper curve). These curves represent the superposition of many experimental measurements from many sources. With the exception of Re = 1300, the measured values from the present study compare well with the plotted vibrating cylinder results.

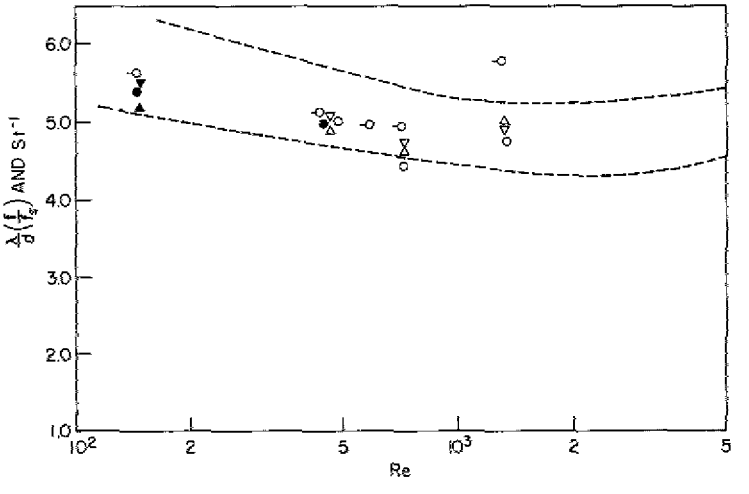

Fig. 8 — Experimental longitudinal vortex spacing λ and reciprocal Strouhal number St^{-1} as a function of Reynolds number in the wakes of vibrating cables (open symbols) and cylinders (solid symbols). The λ measurements are for $f = f_s$ (circles), $f = 0.9f_s$ (triangles with apex upward), and $f = 1.1f_s$ (triangles with apex downward). The dashed lines denote bounds for St^{-1} from Chen [16], and the symbol denotes St^{-1} from the present experiment.

Table 2 — Vortex Spacing and Convection Speed in the Wakes of Vibrating Cables (values determined by applying Eq. (2) to data shown in Fig. 8)

Reynolds Number Re	Ratio of Maximum Amplitude to Cable Diameter $a(0)/d$	Ratio of Vibration Frequency to Strouhal Frequency f/f_s	Ratio of Vortex Spacing to Cable Diameter λ/d	Ratio of Convection and Free Stream Velocities U_φ/U_0
470	0.2	0.9	5.38	0.89
	0.2	1.0	5.08	0.92
	0.2	1.1	4.60	0.91
570	0.3	0.92	5.22	0.89
715	0.2	0.9	5.20	0.88
	0.2	1.0	4.70	0.88
	0.2	1.1	4.00	0.82
1300	0.2	0.9	5.44	0.79
	0.2	1.0	4.96	0.80
	0.2	1.1	4.28	0.76

The results in Table 2 and Fig. 8 were all obtained directly downstream from a cable antinode. Similar measurements made at various other locations along the cable span, for $a(0)/d = 0.3$, $f/f_s = 0.92$, and Re = 570, are plotted in Fig. 9. Since the analog correlation function can respond only to a fluctuation with some regularity in phase, there is no coherent vortex structure behind the nodal area until $z < 0.18L$, where L is the cable vibration wavelength. The critical amplitude at this frequency for a rigid cylinder occurs at $z = 0.2L$; thus this finding is consistent with the results in the previous section. More importantly the vortex spacing for $0 < z < 0.18L$ can be obtained directly from the figure. Once the coherent structure is established, the vortex spacing is constant across the wake, and this results in a constant induced street velocity at which the vortex filaments are convected downstream. Figure 9 also suggests that the irregular wake area downstream from the node is interacting with the downstream portions of the wake adjacent to it. This spreading of the irregular nodal wake flow has been observed in a related flow-visualization study of the wakes of vibrating cables in water [17]. The correlation function in Fig. 9 is not normalized, so that the large increase in magnitude approaching the antinode is a consequence of higher velocity fluctuations rather than such a large improvement in the correlation of the vortex shedding.

Until now the wake behind the vibrating cable has been considered as two regimes consisting of a synchronized or locked-in segment about the antinode and an unsynchronized segment about the node. However the unsynchronized segment can be further divided according to the wake structure. The fluctuating velocity spectra downstream from the nodes in each case contain essentially a single peak at the Strouhal shedding frequency. This suggests that the wake structure in the immediate vicinity of the node of a vibrating cable is much like that of a stationary cable. This supposition was verified by flow visualization, and the resulting photographs in Fig. 10 were taken at Re = 570 with the cable vibrating at the conditions $a(0) = 0.3d$ and $f = 0.92f_s$. Two photographs were taken at each location and each pair consists of a stationary-cable wake condition

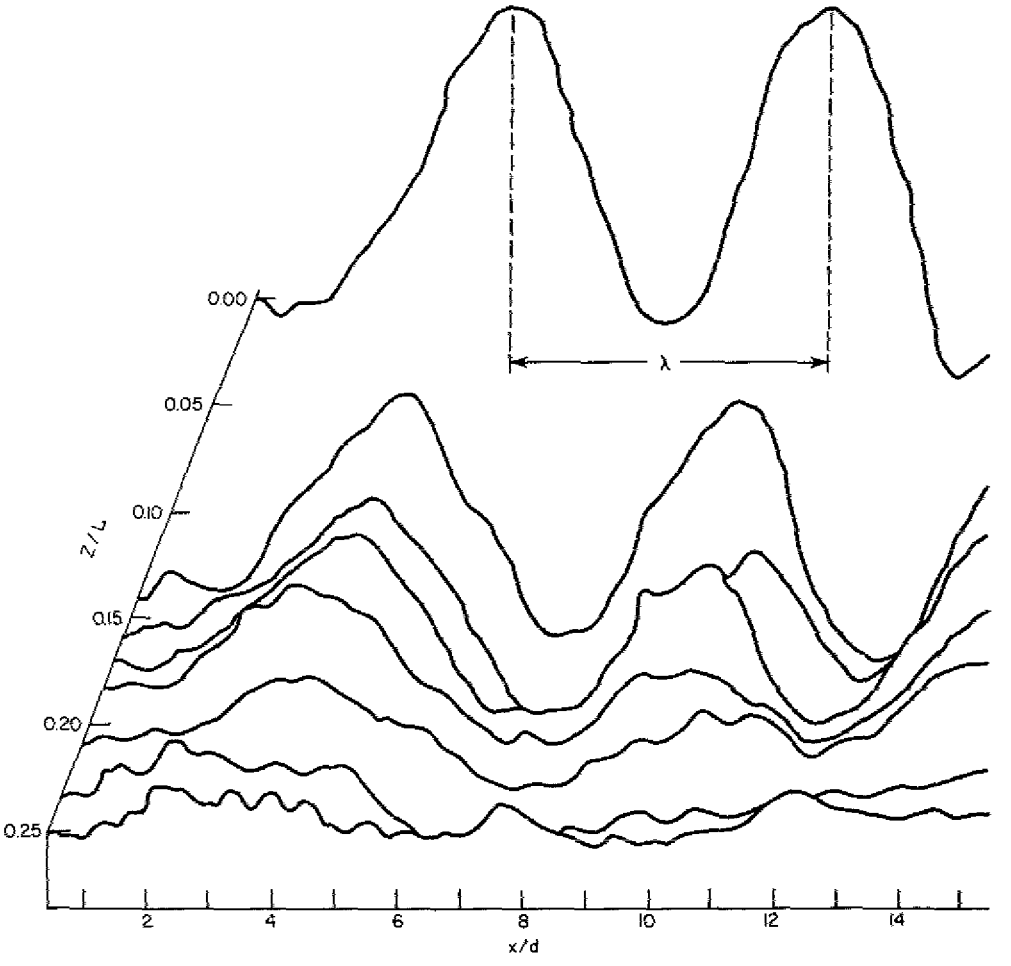

Fig. 9 — Several streamwise correlograms at various locations along the cable span for $a(0)/d = 0.3$, $f/f_s = 0.92$, and Re = 570

and the analogous vibrating-cable wake condition. For reference purposes each stationary-cable photograph in the left column represents the same flow conditions as the corresponding member of the right column.

Near the node (photographs for $z = 0.25L$ and $0.24L$ and $a/d = 0.0$ and 0.02) the two vibrating-cable wake geometries are essentially the same as those of the corresponding stationary cable. The vortex spacings for the two cases were computed, and for these first two positions the ratios are 0.99 and 1.00, which confirms the similarity in structure. Further along the cable where the amplitude is larger ($a/d = 0.09$) but still below the lock-in threshold, the Strouhal shedding structure is modified beyond recognition by the cable vibration. This wake flow is also unsynchronized and could be termed a transition regime the stationary body flow near the node and the wake capture at the higher amplitudes.

The correlograms of Fig. 9 were obtained under nearly identical conditions and compare well with the flow visualization results. Since the correlation contains some averaging and the pictures are instantaneous records, it follows that two distinct wake structures exist in the unsynchronized region associated with a cable node. The correlograms suggest the existence of frequency locking for $z < 0.18L$, and this also follows

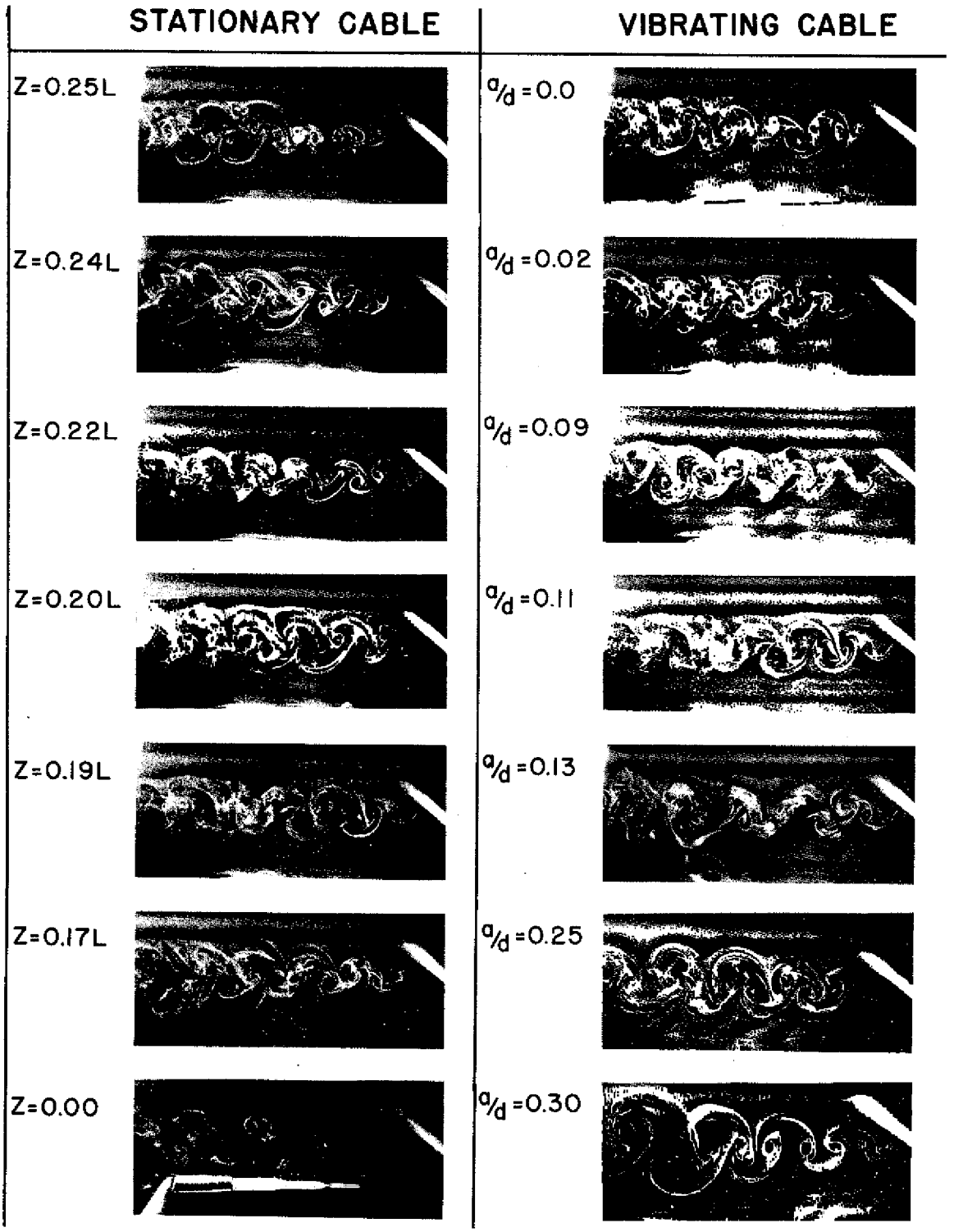

Fig. 10 — Flow visualization of several locations along a stationary cable and a vibrating cable at Re = 570. One cable was vibrating at $f = 0.92f_s$ with an antinode amplitude of 30% of a diameter peak-to-peak.

from an examination of the last four photographs of the vibrating cable wake. The wakes at a/d = 0.11 and a/d = 0.13 are somewhat ragged and reflect the boundary region of the locked-in shedding, but the measured vortex spacing ratios of the last four photographs (0.91, 0.93, 0.94, and 0.91) suggest that a single synchronized wake structure is present. Lastly, the strobe light system, flashing at the vibration frequency, began to freeze the wake at about $z = 0.18L$, and this yields further evidence of the initiation of the locking-in.

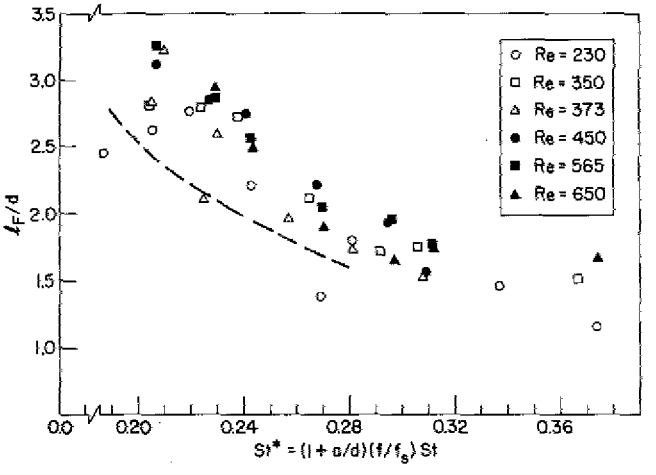

Fig. 11 — Formation length ℓ_F downstream from a cable antinode as a function of the wake-capture Strouhal number St* (from Ref. 13). The dashed line represents measurements made behind cylinders.

The final vibrating-cable photograph is comparable in character and regularity to the previous visualization [1,5,15] of locked-in vortex shedding from rigid cylinders at lower Reynolds numbers. On the other hand the stationary-cable photographs contain evidence of turbulence effects not present in the photographs of the vortices at the lower Reynolds numbers. An important feature to note in the photographs of Fig. 10 is the apparent suppression of the turbulence for the locked-in shedding from the cable at Re = 570. This effect has been observed previously but not for flexible bodies or at Reynolds numbers beyond 350. The apparent suppression of turbulent effects will be used in the modeling of the vortex wake that is discussed in the following sections.

THE VELOCITY FIELD OF THE CABLE WAKE

In the recent examination [13,14] of the vortex formation and early wake development behind a vibrating cable, the authors measured the length of the vortex formation region over a wide range of Reynolds numbers and vibration parameters within the regime of wake capture or lock-in, since there is a close relation between changes in the formation region flow and changes in the lift, drag, and base pressure on bluff bodies [13,18]. These measurements are summarized in Fig. 11, and the decrease in formation length ℓ_F with St* is indicative of the increased fluid forces which accompany different vibration conditions. The parameter St* is a wake-capture or frequency-locking Strouhal number based on the vibration (and vortex) frequency f, a characteristic length $(a + d)$, and the undisturbed fluid velocity U_0.

These experiments also showed that the formation length and consequently the fluid forces depend on the frequency and the *local* amplitude in the wake of a cable, thus suggesting a local relationship between the flow-induced forces and the cable motion. To determine a relation between the hydrodynamic parameters of the wake and the vibrations, it is necessary to match a model for the vortex street with measured velocity profiles.

A difficult problem arises however during any attempt to systematically compare the properties of vortex-street wakes under different flow conditions, because the measurements depend on the relative distance from the point at which the vortices are formed, that is, on the formation length ℓ_F. This problem is compounded when any changes are made in the mechanism of the vortex shedding. Such changes may include mass addition and splitter plates in the base region of a bluff body or may include the flow-induced and forced oscillations of structures and taut cables. Such a problem arises in the present case because the formation region at, for example, Re = 450 is reduced in length from 3.1 to 1.6 diameters as the amplitude of vibration is increased from zero to half a diameter, and any interpretations based on wake measurements made at an arbitrary downstream value of x/d can be seriously misleading. The wake of a cable is complicated still further in that the amplitude of oscillation varies along the cable span. As shown in the previous sections, this results in a portion of the cable wake where the vortex and vibration frequencies are fully synchronized, a portion where the amplitude is just below the lock-in threshold, and finally the flow field downstream from the cable's node.

The rms and mean velocity distributions downstream of a cable antinode are illustrated in Figs. 12a and 12b respectively for some typical examples of the cable wake flow patterns under study here. The velocity distributions in the figures, measured downstream from the antinode of a vibrating cable, illustrate the development of vortex wake flow behind a bluff body, which is described in detail elsewhere in the literature [2,5,10,14,15]. A model for the vortex street, described in the next section, was employed to determine the vortex strength, age, and spacing, and from these findings the vortex-induced drag was computed. The initiation of the early turbulent wake appears to be suppressed by the vibrations at these Reynolds numbers between 400 and 600, thereby making possible the use of the wake model which was previously used for a similar study at a lower Reynolds number of 144 [15].

A MATHEMATICAL MODEL FOR THE VORTEX STREET

The downstream portion of the vortex wake of a cable offers suitable locations at which to measure the strength, age, and spacing of the vortices, with due regard being given to the constraints which were outlined in the previous section. To account for the finite core radii of the real vortices, the potential vortices at an abritrary number of positions in the classical vortex-street model can be replaced by Hamel-Oseen vortices. The circumferential velocity and vorticity fields of such viscous vortices are respectively

$$u_\theta = \frac{K}{2\pi r}\left[1 - e^{-1.26(r/r_*)^2}\right], \qquad r_*^2 = 5.04\,\nu t, \tag{3a}$$

and

$$\zeta = \frac{1.26K}{\pi r_*^2}\, e^{-1.26(r/r_*)^2}, \tag{3b}$$

where r_* represents the radial distance from the vortex center to the maximum of u_θ, t is the age of the vortex, and K is the initial circulation. The basic von Karman vortex street, corrected in this way for the effects of viscosity, should be an appropriate model for the vibrating cable wake, since the flow, at least in the frequency-locking regime, is governed by local values of vibration amplitude and frequency.

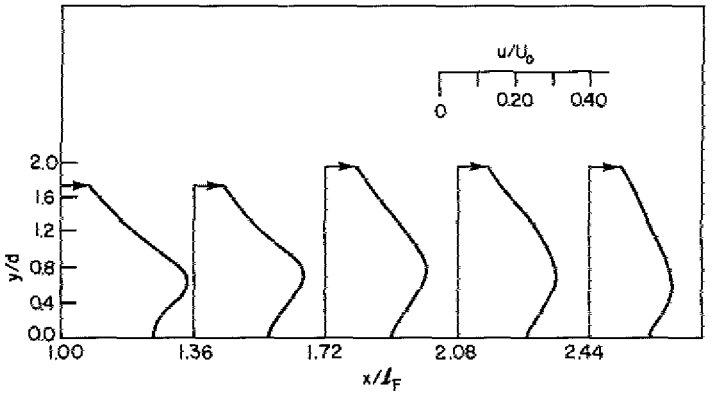

(a) — Root-mean-square fluctuating velocity distribution

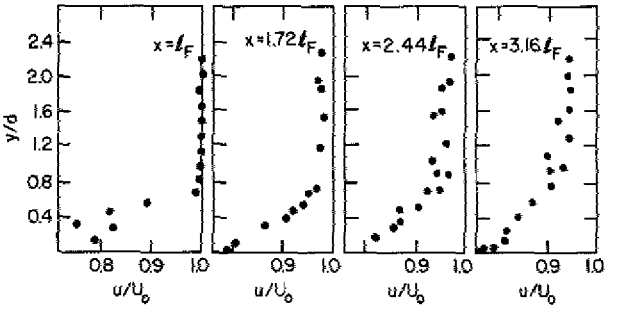

(b) — Mean velocity distribution

Fig. 12 — Velocity distributions downstream from a cable antinode for Re = 450, $f/f_s = 1.0$, and $a/d = 0.3$

The complex velocity potential for an inviscid street of vortices, taken at some initial time $t = 0$ and in coordinates (Fig. 13) fixed relative to the equilibrium position of the cable, is

$$\psi = \frac{iK}{2\pi} \ln \frac{\sin\left[\pi(z' - z_0')\right]}{\sin\left[\pi(z' + z_0')\right]} + U_0 \lambda z',$$

where $z' = z/\lambda = \xi + i\eta$ and $z_0' = (1/4) + i\mu$. At this initial time the vortices in the upper row are at the positions $m + (1/4) + i\mu$ and the vortices in the lower row are at the positions $m - (1/4) - i\mu$, for $m = 0, \pm 1, \pm 2$, etc. The velocity components are given by

$$u_{\text{pot}} - iv_{\text{pot}} = \frac{d\psi}{dz},$$

where $z = \lambda z'$. The results are

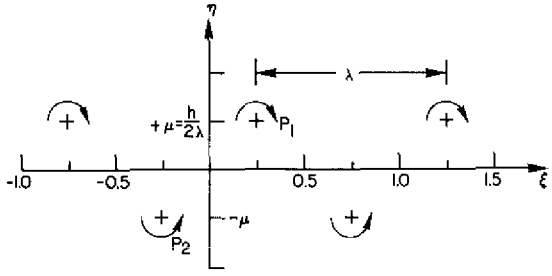

Fig. 13 — Coordinate system for an infinite vortex street with constant lateral spacing h and longitudinal spacing λ. The vortices P_1 and P_2 are replaced by Hamel-Oseen viscous vortices in determining the velocity components given below.

$$\frac{u'}{U_0}(x', y') = 1 - \left(\frac{K}{U_0\lambda}\right) \frac{\cosh 2\pi\mu\,(\sinh 2\pi\mu - \sin 2\pi\xi \sinh 2\pi\eta)}{(\sinh^2 2\pi\mu + \sinh^2 2\pi\eta + \cos^2 2\pi\xi - 2\sinh 2\pi\mu \sin 2\pi\xi \sinh 2\pi\eta)}$$

$$- \frac{K}{2\pi U_0\lambda} \frac{\exp\left\{-\alpha\left[\left(\xi - \frac{1}{4}\right)^2 + (\eta - \mu)^2\right]\right\}}{\left[\left(\xi - \frac{1}{4}\right)^2 + (\eta - \mu)^2\right]} (\eta - \mu)$$

$$+ \left(\frac{K}{2\pi U_0\lambda}\right) \frac{\exp\left\{-\alpha\left[\left(\xi + \frac{1}{4}\right)^2 + (\eta + \mu)^2\right]\right\}}{\left[\left(\xi + \frac{1}{4}\right)^2 + (\eta + \mu)^2\right]} (\eta + \mu), \tag{4a}$$

$$\frac{v'}{U_0}(x', y') = \left(\frac{K}{U_0\lambda}\right) \frac{\cosh 2\pi\mu \cos 2\pi\xi \cosh 2\pi\eta}{(\sinh^2 2\pi\mu + \sinh^2 2\pi\eta + \cos^2 2\pi\xi - 2\sinh 2\pi\mu \sin 2\pi\xi \sinh 2\pi\eta)}$$

$$+ \left(\frac{K}{2\pi U_0\lambda}\right) \frac{\exp\left\{-\alpha\left[\left(\xi - \frac{1}{4}\right)^2 + (\eta - \mu)^2\right]\right\}}{\left[\left(\xi - \frac{1}{4}\right)^2 + (\eta - \mu)^2\right]} \left(\xi - \frac{1}{4}\right)$$

$$- \left(\frac{K}{2\pi U_0\lambda}\right) \frac{\exp\left\{-\alpha\left[\left(\xi + \frac{1}{4}\right)^2 + (\eta + \mu)^2\right]\right\}}{\left[\left(\xi + \frac{1}{4}\right)^2 + (\eta + \mu)^2\right]} \left(\xi + \frac{1}{4}\right), \tag{4b}$$

$$\left(\frac{q'}{U_0}\right)^2 = \left(\frac{u'}{U_0}\right)^2 + \left(\frac{v'}{U_0}\right)^2, \tag{4c}$$

and

$$\lim_{\substack{\eta\to\mu \\ \xi\to 1/4}} \left(\frac{q'}{U_0}\right) = \frac{f\lambda}{U_0} = \frac{U_\varphi}{U_0}. \tag{4d}$$

In these equations

$$\mu = \frac{h}{2\lambda}, \quad \alpha = \frac{\lambda^2}{4\nu t}, \quad \xi = \frac{x'}{\lambda} \text{ and } \eta = \frac{y'}{\lambda}$$

within the range

$$-0.5 \leqslant \xi \leqslant 0.5, \eta \geqslant 0.$$

These results represent those finally obtained with only the potential vortices at the positions P_1 and P_2 replaced by viscous vortices, since the replacement of others was subsequently found to be unnecessary in these and related computations [15,18]. Some recent results of Chaplin [19] have shown that two Hamel-Oseen vortices are sufficient for small values of the vortex core radius, $r_* < 0.3\lambda$, and the results discussed in the next section fall within this range.

Several assumptions are inherent in the preceding use of the vortex-street model. The core radius r_* or age t is assumed to be constant as the street moves over one cycle; thus the results represent an average value of r_* or t at a given downstream displacement. Likewise the transverse spacing h of the vortices is constant in the mathematical formulation, and this assumption has been shown to be valid in the downstream region of the wake where the lateral motion of the vortex centers is small. The finite length of the real vortex street for $x > 0$ is also disregarded in the formulation, and this approximation has also shown to be acceptable [15,18], since in the region of matching the lateral motion of the vortices is small. Weihs [20] has recently shown that a vortex-street model with constant lateral spacing has considerable utility as an initial step toward further understanding of the interaction between a vibrating bluff body and its wake.

The velocity distribution given by Eqs. (4) has been used to evaluate the vortex-street parameters at several axial positions along the cable's half-wavelength and at several downstream positions at each of these axial stations. Four unknown parameters are to be evaluated: the vortex strength $K/2\pi$ (in units of m^2/s), where K is the initial circulation, the core radius r_* (m), the lateral spacing h (m), and the longitudinal spacing λ (m). The last, λ, was measured directly. The three remaining parameters are determined here from the experimental velocity profiles by matching the measured and computed mean and rms velocity profiles at nine equally spaced lateral displacements between 0 and $2d$ from

the centerline of the wake. The solution is then chosen as the set of parameters K, r_*, and h/λ that results in a minimum of the error function

$$E = \sum_{j=1}^{9} \left(\frac{u_{m,j} - u_{c,j}}{u_{m,j}} \right)^2 + \left(\frac{U_{m,j} - U_{c,j}}{U_{m,j}} \right)^2 . \tag{5}$$

A related criterion was successfully employed by the authors in an earlier study of the circular-cylinder wake [15,18] which also included some preliminary results obtained for the wake of a cable. The computed velocities u_c and U_c are obtained by sweeping through a cycle of the vortex street from $\xi = -0.5$ to $\xi = 0.5$, for chosen values of K, r_*, and h/λ, after which the total mean and rms velocities based on both the u and v components are computed at each value of y. The coordinate $\xi = 0$ then corresponds to the downstream position of the matching between theory and experiment.

MODEL COMPUTATIONS OF VORTEX STRENGTH AND SPACING

The computations involved in matching the experimental data with the model are time consuming, but they can be readily carried out on a digital computer. At each of the chosen values of y/d the velocity $q = (u'^2 + v'^2)^{1/2}$ was determined for chosen values of r_* and h/λ over 100 steps in the interval $-0.5 < \xi < 0.5$, and the local mean and rms velocities were computed. An initial guess at K also was necessary, but the solution quickly converged, and two successive average values of K at all the points were obtained to within an arbitrary K/K_{av}, say 10^{-3}. Thus a particular triplet of the parameters K, r_*, and h/λ resulted in a certain error E as given by Eq. (5), and the solution was defined as the set of parameters that yielded the minimum error. Some examples are given in Figs. 14 and 15 to indicate the agreement in the lock-in regime between the measured cable-wake velocity profiles and those generated on the computer. The agreement is comparable to that which was obtained in a recent study of the wake of a vibrating cylinder [15], for both the rms and mean velocity profiles.

The vortex strength should remain constant over a finite downstream distance in order for the street model to be an optimum approximation for the real wake. The results listed in Table 3 indicate that this criterion is satisfied to an acceptable degree in the present study. Not only does the vortex strength remain virtually constant, but the lateral spacing of the vortices increases only slightly with downstream distance. The vortex-strength (circulation) results indicate an increased wake strength in response to the vibrations, and the proportionate increase is similar to what one might expect from available vibrating-cylinder results [15]. For instance, when the wake and cable frequencies are completely locked in with each other at Re = 570 and at $f = 0.92f_s$, there is an increase of 39% from the stationary-cable value ($K/\pi U_0 d = 0.64$) when the amplitude is 24% of a diameter.

When the wake behind the cable segment vibrating at 8% of a diameter is considered, the results are more complicated. The results in Figs. 5b and 9 show little discernible coherence in the downstream shedding at this amplitude, and the wake energy is concentrated near the component C_n at the vibration frequency f. A matching between the measured velocity profiles and the vortex-street model was made at two values of

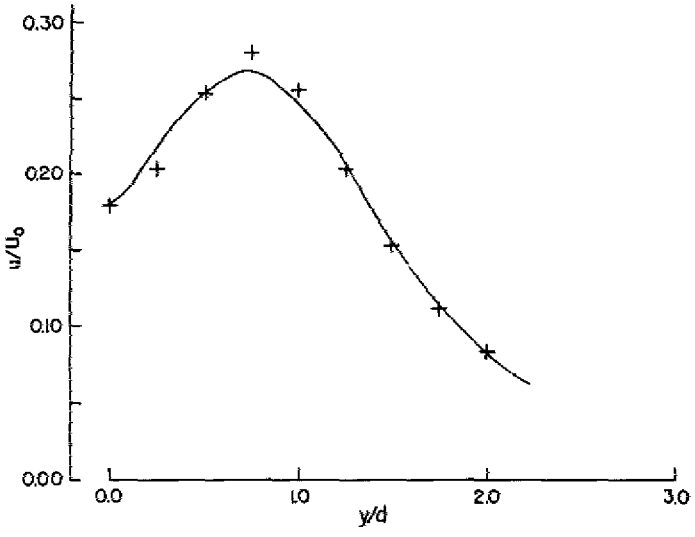

(a) — $f = f_s$, $a = 0.3d$, $x = 4.6d$, and Re = 450

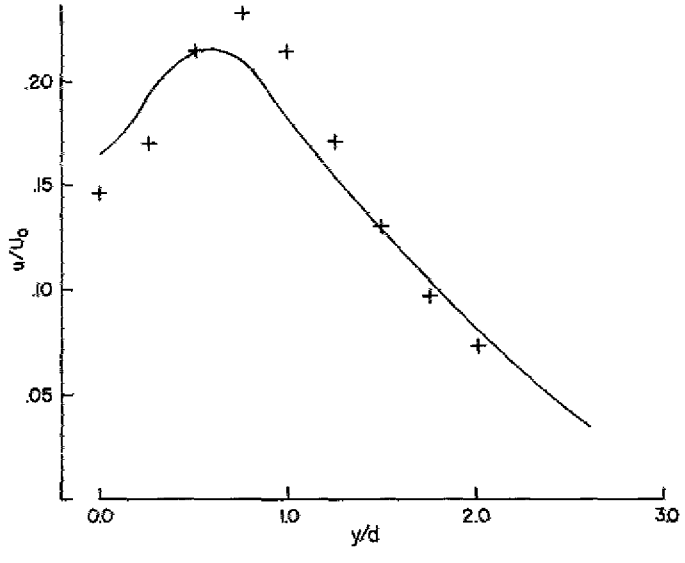

(b) — $f = 0.92f_s$, $a = 0.24d$, $x = 6d$, and Re = 570

Fig. 14 — Measured (curves) and computed (points) root-mean-square velocity profiles in the wake of a vibrating cable

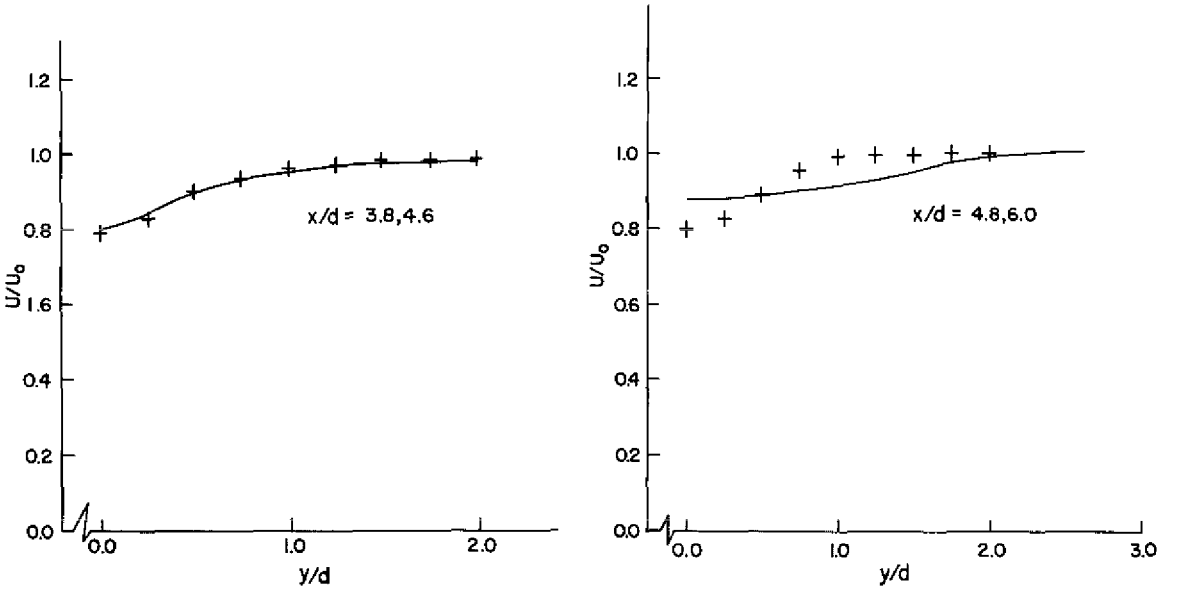

(a) — $f = f_s$, $a = 0.3d$, and Re = 450

(b) — $f = 0.92f_s$, $a = 0.24d$, and Re = 570

Fig. 15 — Measured (curves) and computed (points) mean velocity profiles in the wake of a vibrating cables

Table 3 — Vortex Strength, Spacing, and Drag

a/d	x/d	r_*/λ	h/λ	λ/d	$K/\pi U_0 d$	Von Karman Drag Coefficient C_{DK}
Reynolds number = 570; frequency = $0.92f_s$						
0.0 (cable node)	5.1	0.104	0.16	4.8	0.75	1.05
	6.0	0.110	0.16	—	0.76	—
0.08	5.1	0.091	0.134	5.2	0.75	
			0.150	4.8	0.79	0.94 ($\lambda = 5.2d$)
	6.0	0.095	0.146	5.2	0.76	1.10 ($\lambda = 4.8d$)
			0.160	4.8	0.82	—
0.24	4.8	0.110	0.135	5.2	0.88	1.13
	6.0	0.110	0.137	—	0.87	—
Reynolds number = 450; frequency = f_s						
0.0 (stationary cable)	—	—	0.18	5.0	0.64	0.90
0.30	3.8	0.113	0.14	5.0	1.00	1.49
	4.6	0.115	0.14	—	1.02	—

longitudinal spacing: $\lambda = 4.8d$, which corresponds to the stationary cable, and $\lambda = 5.2d$ for the vibrations of $f = 0.92f_s$. An increase in the vortex strength was obtained for each case, and the spectral content of the wake signal (Fig. 5b) indicates that the vortex strength corresponding to $\lambda = 5.2d$ is the more appropriate of the two values. An additional complication arises in trying to interpret the results in the transition segment of the wake; significant contributions to the spectral content of the near-wake velocities sometimes included not only f and f_s but also a low-frequency peak at the difference of these two frequencies and a high-frequency peak at their sum. Thus, a vortex-street model such as the one employed herein gives only a first approximation to such a complicated flow regime. Bearman and Davies [21], in reporting some experiments to ascertain the lock-in boundaries for various bluff body shapes, also observed the appearance of sum and difference frequencies of f and f_s when lock-in was not complete.

A matching was made also with velocity profiles measured downstream of the cable node ($a = 0$). For this location the spacing was $\lambda = 4.8d$, which corresponds to the stationary cable under the same flow conditions. However the wake strength downstream of the node is somewhat greater than downstream of the stationary cable. The results in Table 3 indicate that the vortex strength $K/\pi U_0 d$ is increased by about 17% from the stationary reference value. This increase in the strength of the wake downstream from the cable's node is possibly a result of interactions with the wakes of nearby vibrating cable segments. Also however the flow-visualization results in the preceding section suggest that the use of the Hamel-Oseen vortex model may be invalid for the nodal region flow at a Reynolds number of 570. Table 3 includes some results obtained when a cable was vibrated at the Strouhal frequency, at a Reynolds number of 450. Again, for vibrations of the cable antinode at 30% of a diameter, the vortex strength $K/\pi U_0 d$ was increased by about 62% from the reference value.

Several further observations can be made in relation to the results contained in Table 3. The lateral spacing of the vortices decreases as the amplitude of vibration is increased at a fixed frequency, as had previously been found for rigid cylinders [15]. For instance the spacing ratio h/λ is decreased from 0.16 to 0.14 as the half wavelength of the cable is traversed at $f = 0.92f_s$ from the nodal region to an amplitude of $0.24d$. A similar decrease in spacing ratio was also found when the cable was vibrating at the Strouhal frequency for a Reynolds number of 450.

The values of the vortex core radius r_* obtained from the matching generally fall between $0.5d$ and $0.6d$ for the experiments at Reynolds numbers of 450 and 570 and can be contrasted with typical results of $r_* \approx d$ at the lower Reynolds number of 144 [15]. The smaller core radii at the higher Reynolds numbers indicate the diminishing importance of the viscous corrections as the Reynolds numbers are increased. Good agreement is obtained however between the Hamel-Oseen correction, Eq. (3), and the experimental velocity profiles even at Reynolds numbers of 450 and 570, which are somewhat beyond the usual range of validity (Reynolds numbers of 200 to 300) for a laminar vortex model. The suppression of turbulence downstream from the cable antinode is probably responsible for the good agreement in the case of the locked-in segment, whereas the increased irregularity in the wake near the node causes the model to be less satisfactory in that region.

VORTEX-INDUCED DRAG

The steady drag force on a bluff body in a uniform stream can be computed by means of the drag formulation which was derived by von Karman and which is discussed in detail by Milne-Thomson [22] and Kochin, Kibel, and Roze [23]. This formulation is based on the following assumptions, which are outlined by Milne-Thomson:

- The wake is composed of point vortices;

- The complex potential will be *nearly* the same as for an infinite street of equally spaced vortices;

- If the cylinder is surrounded by a control volume whose dimensions are large compared with those of the cylinder and with the street spacing, and if this contour advances with the velocity of the vortex street, then the motion on the boundaries will be steady.

- The formation of the vortices is truly periodic.

Although these assumptions may at first glance appear overly restrictive, they are satisfied to a remarkable degree in the wakes of vibrating bluff bodies. In previous related work [15,18] the vortices in the wake at Reynolds numbers of 144 and 450 were corrected for the effects of the vortices' finite cores, but the assumption of point vortices is reasonable, since a typical dimension of the contour which surrounds the cylinder is many times the core radius of a vortex. The radii r_* of the vortex cores were found by the authors to be approximately $0.5d$ to d in the vibrating cylinder and cable wakes [18]. The use of the complex potential for an infinite vortex street neglects the presence of the body but yields good agreement with the velocity field of the wake in the region where the street is fully developed with little lateral motion. Finally the periodic street of vortices is an excellent approximation for the wake of a vibrating bluff body because of the increased two-dimensionality and periodicity in the wake as a result of body vibrations within the lock-in regime.

The configuration just mentioned is illustrated in Fig. 16. In coordinates fixed to the equilibrium position of the body, the undisturbed flow velocity is U_0, and the vortices move downstream with the velocity $f\lambda$, where f is the vibration (and vortex) frequency and λ is the longitudinal spacing. If the contour ABCD is fixed relative to the vortex street and all motions are viewed from that reference frame, then the body of diameter d moves to the left with the velocity $-f\lambda$, the vortex street is stationary, and the fluid far from the wake and ahead of the cylinder has a velocity $U_0 - f\lambda$. This system is dynamically equivalent to the case of uniform flow past the body. When an otherwise stationary bluff body is vibrating in the y direction, the increased vortex drag should be accompanied by changes in the momentum and force balances on the fluid contained within the contour. The steady drag is obtained in the classical development by integrating the instantaneous drag expression over a period of the natural vortex motion; in the case of a vibrating bluff body the period of the integration is equal to the synchronized periods of the vortex street and the body motion.

The resulting vortex drag equation, following the developments of Milne-Thomson [22] and Kochin, Kibel, and Roze [23], is

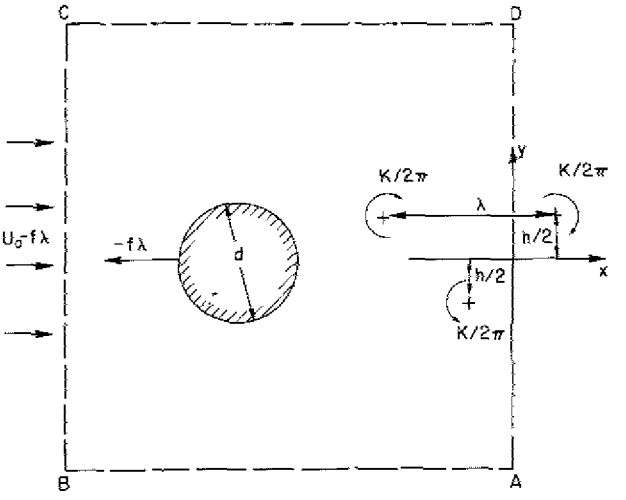

Fig. 16 — The contour ABCD which bounds a control volume containing a cylinder and a vortex street generated by the cylinder. The cylinder oscillates at conditions corresponding to any single point on a flexible cable, and the contour as indicated is fixed relative to the vortices.

$$D = \frac{\rho K^2}{2\pi\lambda} + \frac{\rho K(2f\lambda - U_0)h}{\lambda}, \tag{6}$$

where D is the drag force per unit distance along the body span, K is the initial circulation of the vortices, and h is the lateral spacing of the vortex street. The von Karman drag coefficient C_{DK} then is

$$C_{DK} = \frac{2D}{\rho U_0^2 d} = \pi \left(\frac{K}{\pi U_0 d}\right) \left[\left(\frac{K}{\pi U_0 d}\right)\frac{d}{\lambda} + 2\left(\frac{2f\lambda}{U} - 1\right)\frac{h}{\lambda}\right]. \tag{7}$$

This same equation was obtained by Synge [24] in his computation of the steady vortex drag on a bluff body. Synge however obtained his version of Eq. (7) after assuming that the fully developed vortex street was made up of a *semi-infinite* street of point vortices with constant lateral and longitudinal spacings. The results obtained with the von Karman drag model will now be discussed for the particular case of a vibrating flexible cable. These results obtained from the wake of a cable will then be compared with available results obtained with vibrating rigid cylinders.

SOME COMPARISONS WITH THE DRAG ON VIBRATING CYLINDERS

The von Karman drag coefficients C_{DK} listed in Table 3 were determined by using Eq. (7), and for all of the results listed higher drag coefficients were obtained relative to a stationary cylinder or cable under similar flow conditions. For example, at Re = 450 the antinodal region of the cable's wake had a von Karman drag coefficient C_{DK} = 1.49,

which is about 65% greater than the corresponding stationary-cable value ($C_{DK,0}$ = 0.9). The vibrating cable at Re = 580 and $f = 0.92f_s$ also resulted in a higher vortex-induced drag coefficient of C_{DK} = 1.13, or an increase of 25% from the stationary-cable value. For both of these experiments the amplitude of vibration was above the threshold for locking-in of the vortex and vibration frequencies.

The drag results obtained at the cable node and at an amplitude of $a = 0.08d$ are not so straightforward, though both indicate an increase in drag corresponding to the increased strength of the wake. The ambiguity in the vortex longitudinal spacing at $a = 0.08d$ results in an ambiguity in the drag coefficient at that location, though increased drag and an increased wake strength are clearly indicated. The results obtained in the region of the cable's node also suggest an increase in the drag and the wake strength from the stationary cable wake. However virtually no coherence in the downstream velocity signals was found in the nodal region (Fig. 9), and the drag coefficient calculated with Eq. (7) can give only an "equivalent" value of vortex-induced drag.

It is useful to obtain a further measure of the von Karman drag behavior by means of a comparison with direct measurements of the drag on vibrating circular cylinders. Tanida, Okajima, and Watanabe [25] recently measured the drag on a vibrating cylinder for a wide range of experimental conditions at Reynolds numbers of 80 and 4000. In their experiments a cylinder was towed through still water in a tank and vibrated at frequencies both in and out of the lock-in regime, and both transverse to and in-line with the tow direction. Direct measurements of the drag on freely vibrating rigid cylinders have also recently been reported by Griffin, Skop, and Koopmann [26] and by Diana and Falco [27]. These measured force results are compared with the vortex-induced von Karman drag coefficients from Table 3 in Fig. 17, where the drag results (normalized by corresponding stationary-cylinder and cable drag values) are plotted as the function of the wake-capture Strouhal number St*. Also plotted in the figure are the results obtained for the vortex circulation K (or strength $K/2\pi$) for both cables and cylinders. The pertinent information necessary to describe the data in Fig. 17 is listed in Table 4.

The most important result shown in Fig. 17 is the correspondence between the increased wake strength and drag forces as a bluff body such as a cable or cylinder undergoes vortex-induced resonant oscillations or is forced to vibrate in the lock-in regime. This increase in the drag on a vibrating bluff body is largely a result of the increased vortex strength in the wake, since a decrease in the lateral spacing of the vortices generally corresponds to a decrease in drag. For all conditions illustrated by the data plotted in the figure a drag amplification of up to 80% is shown to accompany the vibrations. Also, the results illustrate an insensitivity to Reynolds number effects once a body is resonantly vibrating. The results of Griffin and Ramberg [18] span the range of Re from 144 to 570, and those of Tanida, Okajima, and Watanabe [25] were obtained at Re = 80 and 4000. The drag measurements for a freely vibrating cylinder reported by Griffin, Skop, and Koopmann [26] were made at Re between 500 and 900, and those of Diana and Falco [27] were made at Re between 2000 and 60,000. Thus the drag amplification and wake response of bluff bodies such as taut cables and cylinders are largely independent of Reynolds number when these structures vibrate under conditions of lock-in.

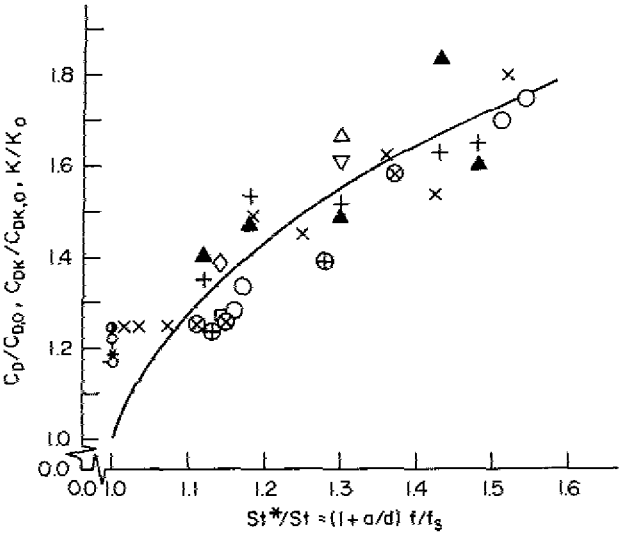

Fig. 17 — The von Karman drag coefficient C_{DK}, the vortex circulation K, and the drag coefficient C_D from direct measurement as a function of the normalized wake parameter St*/St. The legend for the data points is given in Table 4.

Table 4 — Legend for Experimental Vortex-Strength and Drag Data in Fig. 17

Symbol	Parameter	a/d	Reynolds Number Re	Strouhal Number St	Investigators
			Cable		
◇	K/K_0	0.24	570	0.21	Present study
◑	K/K_0	0.08	570	0.21	Present study
*	K/K_0	Node	570	0.21	Present study
△	K/K_0	0.30	450	0.21	Griffin and Ramberg [18]
□	$C_{DK}/C_{DK,0}$	0.24	570	0.21	Present study
♀	$C_{DK}/C_{DK,0}$	0.08	570	0.21	Present study
-○	$C_{DK}/C_{DK,0}$	Node	570	0.21	Present study
▽	$C_{DK}/C_{DK,0}$	0.30	450	0.21	Griffin and Ramberg [18]
			Rigid Cylinder, Forced Vibration		
+	K/K_0	—	144	0.18	Griffin and Ramberg [18]
▲	$C_{DK}/C_{DK,0}$	—	144	0.18	Griffin and Ramberg [18]
⊗	$C_D/C_{D,0}$	—	80	0.14	Tanida, Okajima, and Watanabe [25]
⊕	$C_D/C_{D,0}$	—	4000	0.18	Tanida, Okajima, and Watanabe [25]
			Rigid Cylinder, Freely Vibrating		
○	$C_D/C_{D,0}$	—	500-900	0.21	Griffin, Skop, and Koopmann [26]
×	$C_D/C_{D,0}$	—	2000-60,000	0.19	Diana and Falco [27]

SUMMARY AND CONCLUDING REMARKS

This report has examined the vortex wake flow of a vibrating flexible cable in the Reynolds number range 470 to 1300. As a result of measurements of velocity correlations and spectra in the flow, measurements of velocity profiles, and flow visualization, three distinct flow regimes have been identified along the cable span.

In the immediate vicinity of a cable node the flow closely resembles that past a stationary body, the velocity fluctuations in the near wake occur principally at the Strouhal frequency, and there is little or no spanwise coherence in the vortex shedding. Consequently time-dependent fluid forces which result from this shedding process are not likely to contribute to the vortex-induced motions of the cable.

Adjacent to the nodal region and extending to the region where the vortex shedding frequency is captured by the cable motion is a transition region wherein the spanwise correlation in the shedding begins to increase. There are major fluctuating velocity components at both the Strouhal frequency and the body vibration frequency within this second region, as well as lesser contributions at the sum and difference frequencies of the two major components. Flow visualization has revealed an irregular vortex pattern which is not identified with the vortex geometries characteristic either of the stationary cable or of a cable vibrating in synchronism with its wake. The time-dependent fluid forces acting on this segment contain several frequency components, but based on the correlation measurements presented here only the component at the vibration frequency contributes significantly to the motion.

A third regime exists in the portion of the flow centered at the cable antinode, and this regime is the one in which the vortex shedding is locked into the cable vibration frequency. The character and the extent of this regime have been studied previously by the authors [13,14]. The correlation in the shedding is high ($\rho \approx 0.9$) in this region, and the spectral content is dominated by a sharp peak at the vibration frequency. The amplitude of this spectral peak is distributed axially in the same sinusoidal distribution as the cable's amplitude of vibration. There is a direct correspondence between the vortex wake at any point in this regime and the wake of a rigid cylinder vibrating at the same Reynolds number, frequency, and local amplitude. Moreover the extent of this region can be closely approximated by the boundaries of the lock-in regime previously found for rigid cylinders. This approximation was examined here by means of vortex coherence and spectral measurements, and its validity was confirmed under conditions for which vortex-induced transverse "strumming" vibrations of cables are likely to occur.

Downstream velocity profiles and the measured longitudinal vortex spacing were matched with a mathematical model for the vortex street to determine the strength and lateral spacing of the vortex street. These parameters were obtained by satisfying a minimum-error criterion previously employed with success by the authors [15]. As in the case of a vibrating rigid cylinder the lateral spacing of the vortex street decreases with increasing amplitude of cable vibration and is unaffected by changes in frequency of oscillation. Meanwhile the longitudinal vortex spacing varies inversely with vibration frequency and is independent of amplitude in the regime where the body and wake frequencies are synchronized.

An inverse relation was found between the vortex strength (initial circulation) and the length of the formation region. This is also in agreement with previous results for vibrating cylinders. The use of a simple vortex model was shown to be appropriate for the locked-in regime of the cable wake due to the apparent suppression of turbulence by the synchronization of the vortex shedding and motion.

The von Karman drag formula was employed to compute the steady drag on the vibrating cables. Once again an inverse relation was found between the steady drag coefficient and the length of vortex formation behind the cable. This result further confirms the close relation, previously shown [18], between changes in the flow-induced forces and changes in the wake flow which accompany the vibrations. Moreover, since the length of vortex formation varies along the span and inversely reflects the amplitude distribution, the steady drag is distributed sinusoidally over most of the cable. The only exceptions are near the nodes, where the steady drag approaches the stationary-cable value. In this report the computed steady drag was increased by the vibrations as much as 65% from the stationary-cable value. The computed steady drag coefficients for the vibrating cable were found to be in good agreement with direct force measurements on vibrating cylinders and cables.

The time-dependent (fluctuating lift and drag) fluid force distributions can be inferred from the results of this report. For modeling purposes one is most interested in the components that contribute to the cable motion. It would thus seem reasonable to expect these components to be distributed in the same manner as the amplitude of motion as a result of the spectral measurements and vortex-strength computations. That is to say, the time-dependent forces possess a pure mode form. According to the correlation measurements however such a model will overestimate the actual forces in direct relation to the extent of the transition regime relative to the extent of the locking-in over a cable's half-wavelength. For typical cable strumming amplitudes ($a(0)/d \approx 1$) the transition regime will be relatively short, and one can estimate that the assumption of only a pure mode distribution overpredicts the cable response by less than 3 percent. (Such an estimate can be obtained by crudely accounting for the presence of transition regimes and comparing the work done per cycle to that of a pure mode distribution.) However pure a mode distribution is certainly simpler to implement and yields a slightly conservative estimate of the cable's response.

REFERENCES

1. G.H. Koopmann, "The Vortex Wakes of Vibrating Cylinders at Low Reynolds Numbers," *J. Fluid Mechanics* 28, 501-512 (1967).
2. O.M. Griffin, "The Unsteady Wake of an Oscillating Cylinder at Low Reynolds Numbers," *J. Applied Mechanics, Trans. ASME*, 38, 729-738 (Dec. 1971).
3. N. Ferguson and G.V. Parkinson, "Surface and Wake Flow Phenomena of the Vortex-Excited Oscillations of Circular Cylinder," *Trans. ASME, J. Engineering for Industry* Series B89 (No. 4), 831-838 (Nov. 1967).
4. G.H. Toebes, "The Unsteady Flow and Wake Near an Oscillating Cylinder," *Trans. ASME, J. Basic Engineering* D91 (No. 3), 493-505 (Sept. 1969).

5. O.M. Griffin and C.W. Votaw, "The Vortex Street in the Wake of a Vibrating Cylinder," *J. Fluid Mechanics* 55, 31-48 (1972).

6. O.M. Griffin, "Flow Near Self-Excited and Forced Vibrating Circular Cylinders," *Trans. ASME, J. Engineering for Industry* 94, 539-547 (May 1972).

7. A. Roshko, "On the Development of Turbulent Wakes from Vortex Streets," NACA Report 1191, 1954.

8. M.S. Bloor, "The Transition to Turbulence in the Wake of a Circular Cylinder," *J. Fluid Mechanics* 19, Part 2, 290-304 (1964).

9. M.S. Bloor and J.H. Gerrard, "Measurements on Turbulent Vortices in a Cylinder Wake," *Proc. Royal Soc., London, Series* A294, 319-342 (1966).

10. J.W. Schaefer and S. Eskinazi, "An Analysis of the Vortex Street Generated in a Viscous Fluid," *J. Fluid Mechanics* 6, 241-260 (1959).

11. P.W. Bearman, "Investigation of the Flow Behind a Two-Dimensional Model with a Blunt Trailing Edge and Fitted with Splitter Plates," *J. Fluid Mechanics* 21, Part 2, 241-255 (1965).

12. J.H. Gerrard, "The Mechanics of the Formation Region of Vortices Behind Bluff Bodies," *J. Fluid Mechanics* 25, Part 2, 401-413 (1966).

13. S.E. Ramberg and O.M. Griffin, "Vortex Formation in the Wake of a Vibrating Flexible Cable," *Trans. ASME, J. Fluids Engineering* 96, 317-322 (1974).

14. S.E. Ramberg and O.M. Griffin, "Velocity Correlation and Vortex Spacing in the Wake of a Vibrating Cable," *Trans. ASME, J. Fluids Engineering* 97, in press (1975).

15. O.M. Griffin and S.E. Ramberg, "The Vortex-Street Wakes of Vibrating Cylinders," *J. Fluid Mechanics* 66, 553-576 (1974).

16. Y.N. Chen, "Fluctuating Lift Forces of the Karman Vortex Streets on Single Circular Cylinders and in Tube Bundles: Part I, The Vortex Street Geometry of the Single Circular Cylinder," *Trans. ASME, J. Engineering for Industry* 94, 603-612 (1972).

17. R. Dale, Jr., and R.A. Holler, "Vortex Wakes from Flexible Circular Cylinders at Low Reynolds Numbers," Naval Air Development Center, NADC Report AE-7011, 1970.

18. O.M. Griffin and S.E. Ramberg, "On Vortex Strength and Drag in Bluff Body Wakes," *J. Fluid Mechanics* 69, 721-728 (1975).

19. J.R. Chaplin, in "Discussion of 'Fluctuating Lift Forces of the Karman Vortex Streets on Single Circular Cylinders and in Tube Bundles, Part 2' by Y.N. Chen," *J. Engineering for Industry, Trans. ASME,* Vol. 94, 619-621 (May 1972).

20. D. Weihs, "Semi-Infinite Vortex Trails, and Their Relationship to Oscillating Airfoils," *J. Fluid Mechanics* 54, 679-690 (1972).

21. P.W. Bearman and M.E. Davies, "The Flow About Oscillating Bluff Structures," Proceedings of the Conference on Wind Effects on Building and Structures, London, 1975.

22. L.M. Milne-Thomson, *Theoretical Hydrodynamics,* 4th edition Macmillan, New York, 1960, Ch. 13.

23. N.E. Kochin, I.A. Kibel, and N.V. Roze, *Theoretical Hydromechanics*, Interscience, New York, 1964, Ch. 5.

24. J.L. Synge, "Mathematical Investigation of the Thrust Experienced by a Cylinder, the Motion Being Periodic," *Proc. Royal Irish Academy* **37**, 95-109 (1927).

25. Y. Tanida, A. Okajima, and Y. Watanabe, "Stability of a Circular Cylinder Oscillating in Uniform Flow or in a Wake," *J. Fluid Mechanics* **61**, 769-784 (1973).

26. O.M. Griffin, R.A. Skop, and G.H. Koopmann, "The Vortex-Excited Resonant Vibrations of Circular Cylinders," *J. Sound and Vibration* **31**, 235-249 (1973).

27. G. Diana and M. Falco, "On the Forces Transmitted to a Vibrating Cylinder by a Blowing Fluid (Experimental study and analysis of the phenomenon)," *Mecchanica (J. Italian Assoc. for Theoretical and Applied Mechanics)* **6**, 9-22 (1971).